



Impacts of land cover changes on biogenic emission and its contribution to ozone and secondary organic aerosol in China

Jinlong Ma¹, Shengqiang Zhu¹, Siyu Wang¹, Peng Wang^{2,3,4*}, Jianmin Chen¹, Hongliang Zhang^{1,4,5*}

¹Shanghai Key Laboratory of Atmospheric Particle Pollution and Prevention, Department of Environmental Science and Engineering, Fudan University, Shanghai, China

²Department of Atmospheric and Oceanic Science, Fudan University, Shanghai 200438, China

³Shanghai Frontiers Science Center of Atmosphere—Ocean Interaction, Fudan University, Shanghai 200438, China

⁴IRDR ICoE on Risk Interconnectivity and Governance on Weather/Climate Extremes Impact and Public Health, Fudan University, Shanghai, China

10 ⁵Institute of Eco-Chongming (IEC), Shanghai 200062, China

*Correspondence to: Peng Wang (w_peng@fudan.edu.cn); Hongliang Zhang (zhanghl@fudan.edu.cn)

Abstract. The greening impacts in China led to an increase in natural emissions, which may further aggravate the local burden of secondary organic aerosol and ozone. Thus, a robust natural emissions inventory is crucial for assessing the contribution of biogenic volatile organic compounds (BVOCs) to air quality. However, using different satellites will introduce uncertainties in BVOC estimations. Quantitative analysis is needed for evaluating the accuracy of BVOC estimations and their impacts on air quality. In this study, Model of Emissions of Gases and Aerosols from Nature (MEGAN) v2.1 was used to investigate the impact of different LAI and LC datasets on BVOC emissions in China in 2016 and impacts on O₃ and SOA were evaluated based on the Community Multiscale Air Quality Modelling System (CMAQ). Three LAI satellite datasets of the Global Land Surface Satellite (GLASS), the Moderate Resolution Imaging Spectroradiometer (MODIS) MOD15A2H version 6 (MOD15), and the Copernicus Global Land Service (CGLS), as well as three LC satellite datasets of the MODIS MCD12Q1 LC products, the Copernicus Climate Change Service (C3S) LC products, and the CGLS LC products were used in five parallel experiments (cases: C1-C5). Results show that BVOC emissions in China range from 25.42 to 37.39 Tg in 2016 and are mainly concentrated in central and south-eastern China, with the highest in C5 (using GLASS and CGLS LC) and the least in C4 (using GLASS and C3S LC). According to model validations, C4 is the better choice for estimating BVOC emissions in China compared to other scenarios. In addition, the use of different LAI and LC inputs has a further impact on the concentrations of O₃ and SOA, especially in central and eastern China, where the differences are up to 4.8-6.9 ppb and 5.3-8.4 μg m⁻³ in O₃ and biogenic SOA (BSOA), respectively. Due to the summer monsoon, a large amount of O₃ is also transported from southern China to the Yangtze River Delta (YRD) and North China Plain (NCP), resulting in a large difference in O₃ concentrations between different cases. For example, the O₃ in C1 (using GLASS and MCD12Q1) is 3.6 ppb higher than in C4 in the YRD. Furthermore, isoprene contributes most to BSOA concentrations in China, which is 1-fold higher than monoterpenes and 1.5-fold higher than sesquiterpenes. The BSOA formed by isoprene is the main reason resulting in the difference between C1 and C5.



1 Introduction

35 Volatile organic compounds (VOCs) from both natural and anthropogenic sources play important roles in the formation of
ozone (O_3) and secondary components of fine particulate matter ($PM_{2.5}$) in addition to their adverse health effects (Volkamer
et al., 2006; Laothawornkitkul et al., 2009; Calafapietra et al., 2013). Globally, biogenic VOCs from vegetations (BVOCs) are
the dominant contributor (with ~90% contribution) to VOCs (Fehsenfeld et al., 1992; Guenther et al., 1995). Isoprene,
monoterpenes, and sesquiterpenes are major BVOC species (Guenther et al., 2006; Wang et al., 2018a) with high photo-
chemical reactivity with ozone (O_3), hydroxyl radical (OH), and nitrate radical (NO_3). In addition, changes in emissions of
BVOCs will alter the capacity of a wide range of warming and cooling climate pollutants that can affect climate (Unger, 2014a,
40 b). Consequently, the studies of BVOC emissions and their effects on air quality and climate are of vital significance.

The Model of Emissions of Gases and Aerosols from Nature (MEGAN) is a widely used (Guenther et al., 2012; Zhao et al.,
2016; Emmerson et al., 2018) model to quantify BVOC emissions in different spatial scales (Guenther et al., 1995; Sindelarova
et al., 2014; Zhang et al., 2017; Jiang et al., 2019a; Wang et al., 2021). Global annual inventories of the isoprene emission ranged
45 from 500 to 750 Tg yr⁻¹ (Guenther et al., 2006) and those of monoterpene emissions ranged from 74.4-157 Tg yr⁻¹ (Guenther
et al., 2012; Messina et al., 2016). BVOC emissions also have been estimated in China by various studies and the results showed
that isoprene emissions were 7.17-29.30 Tg yr⁻¹ and monoterpene emissions were 2.83-5.60 Tg yr⁻¹ (Guenther et al., 2006; Fu
and Liao, 2012; Li et al., 2020). In addition to the national scale, the regional BVOC emissions also have been evaluated, such
as Pearl River Delta (PRD), Yangtze River Delta (YRD), and Beijing (Situ et al., 2013; Wang et al., 2018a; Wang et al., 2020).
50 However, there are considerable uncertainties in BVOC estimations due to incomplete information on model inputs, activity
factors, and emission factors (Situ et al., 2014; Guenther et al., 2012). Those factors can influence the accuracy of estimations
and will further result in misunderstanding the impacts on O_3 and SOA. Therefore, it is necessary to quantify the influence
of those factors and determine the bias in BVOC emissions.

55 Land cover (LC), including leaf area index (LAI) and plant function types (PFTs) fractions, is a major factor that affecting the
BVOC emissions in the MEGAN model (Guenther et al., 2006; Pfister et al., 2008; Guenther et al., 2012). There are many LAI
and LC products generated by various satellite sensors with different process methods, spatial and temporal resolutions. These
products show discrepancies in biomass distributions and PFTs fractions which can enlarge bias in BVOC estimations (Leung
et al., 2010; Wang et al., 2020; Opacka et al., 2021). Guenther et al. (2006) reported that differences in isoprene emissions could
60 be 24% and 29% due to changing PFTs and LAI, respectively. Pfister et al. (2008) found that differences in BVOC emissions
were more significant on a regional scale than global by employing three different PFTs and LAI databases to drive the
MEGAN model. Wang et al. (2018a) showed that the differences in BVOC estimations as a result of changing PFTs (35.5%)
and LAI (22.8%). China is a typical greening country across the world with the forest area of 22.96% in 2018 (NFGA, 2019),



65 contributing large annual BVOC emissions to the world (Opacka et al., 2021), and thus reasonable comparisons in LAI and LC satellite products are essential for better understanding China BVOC emissions.

Contributions of BVOCs to surface O₃ and SOA have been evaluated through chemical transport models (CTMs) at different spatial scales (Carlton and Baker, 2011;Fu and Liao, 2014;Jiang et al., 2019b;Zhang et al., 2020). Fu and Liao (2012) used the CTM to quantitate the impact of biogenic emissions on O₃ in China over the year 2001-2006 and found that the difference in O₃ concentrations induced by interannual variability of BVOCs could be 2-5%. Based on the Weather Research and Forecasting model coupled with Chemistry (WRF-Chem), Situ et al. (2013) reported that the effect of isoprene emissions on surface O₃ in urban areas was higher than that of rural areas in the PRD, which was up to 57% approximately. In addition to the impact on surface O₃, Wu et al. (2020) studied the contributions of BVOCs to SOA in China in 2017 by using the Community Multiscale Air Quality (CMAQ) and the result indicated that BVOCs are the main source of the formation of SOA in summer, which was up to 70%. Qin et al. (2018) investigated the biogenic SOA (BSOA) during summertime in 2012 and found that the SOA concentration from the biogenic source was up to ~10 µg·m⁻³ in Sichuan. However, previous studies only focused on the impacts of BVOCs estimated by the specific LAI and LC satellite products on air quality. The uncertainties in BVOC estimations induced by different satellite products also have an impact on O₃ and SOA concentrations. Kim et al. (2014) showed that the different PFTs distributions had a significant impact on hourly and local O₃, which was up to 13 ppb. Wang et al. (2020) evaluated that the impacts on O₃ reached 20% by using different LC datasets in BVOC emissions in the YRD. The influence of these uncertainties on air quality was not well quantified and the bias in air quality remained unclear in China. Therefore, it is necessary to conduct a comprehensive analysis of the influence of different satellite products on BVOC emissions as well as the further impact on air quality.

85 In this study, the objectives are to estimate the difference in BVOC emissions induced by different LAI and LC databases in China and study the effects of differences in BVOC emissions on surface O₃ and SOA concentration in China. We used three LAI satellite datasets and three LC satellite datasets as the MEGANv2.1 input to estimate the BVOC emissions and then coupled results with a source-oriented model to quantify the effect on air quality. Section 2 introduces the MEGAN model, the source-oriented CMAQ model, and datasets. The model performance, BVOC estimations based on different satellite products, as well as the impact of BVOCs on atmospheric pollutants are described in Section 3, while Section 4 concludes the study.

2 Methodology

2.1 Data description

LAI and PFTs are key parameters for BVOC estimations. Three land cover (LC) datasets were applied as PFTs inputs, including the Moderate Resolution Imaging Spectroradiometer (MODIS) MCD12Q1 LC products (Friedl and Sulla-Menasse, 2019), the Copernicus Climate Change Service (C3S) LC products (C3S, 2021), and the Copernicus Global Land Service



(CGLS) LC products (Buchhorn et al., 2020). MCD12Q1 provides yearly global LC maps from 2001 to 2020 with spatial resolution at 500 m, which is widely used in previous studies (Guenther et al., 2006; Wang et al., 2018a; Wu et al., 2020). Thus, MCD12Q1 is chosen as the baseline LC input for MEGANv2.1 to investigate the model performance with different LAI satellite products. Sources of these products were listed in Table S2. These three LC maps were first re-gridded to the WRF
100 grid for getting the area fraction of each LC type and then were classified into 16 PFTs according to the legend descriptions of maps for the model (Wang et al., 2021; Wang et al., 2018a). Fig. 1 shows the simulation domain with the spatial distribution of majority PFTs. All three datasets represent a similar spatial distribution of grass in northwest China, while there are different majority PFTs distributing in the central and southern China. Crop land is the dominant PFT in central and southern China in the C3S LC map. In addition to the distribution of majority PFTs, the density of needleleaf tree is higher in MCD12Q1 products
105 compared to the other datasets. Although MCD12Q1 and CGLS LC both show a large area of broadleaf tree in central and southern China, the area fraction of broadleaf tree in CGLS LC is higher than that in MCD12Q1 (Fig S2).

The Global Land Surface Satellite (GLASS) (Xiao et al., 2014; Xiao et al., 2016), the MODIS MOD15A2H version 6 (MOD15) (Myneni et al., 2015), and the CGLS LAI products (Fuster et al., 2020) were applied as LAI inputs for MEGANv2.1. The
110 spatial resolutions of GLASS, MOD15, and CGLS are 500m, 500m and 300m, respectively, while the temporal resolutions of these three products are 8 days, 8 days, and 10 days, respectively. Sources of these products were listed in Table S2. According to validation results in Xiao et al. (2016), GLASS shows better consistency with LAI maps than MOD15 in high temporal resolution, while CGLS is slightly less accurate than MOD15 (Fuster et al., 2020). Therefore, the GLASS is used as the baseline LAI input. In the MEGAN model, the grid average LAI is divided by the fraction of grid that is covered by vegetation to represent the LAI of vegetation covered surface, which is refer to LAI_v (Guenther et al., 2006). Figure 2 represents the spatial
115 distribution of LAI from three satellite datasets in the summer of 2016. GLASS shows higher LAI_v value in most part of China, especially in southern China, compared to MOD15 and CGLS in summer.

2.2 Model description

An updated source-oriented CTM was applied to determine O₃ and SOA concentrations from BVOCs based on the CMAQ
120 model v5.0.1 (Byun and Schere, 2006). The model utilized a revised SAPRC-11 photochemical mechanism (S11) (Carter and Heo, 2013), which included a more explicit description of isoprene oxidation chemistry to improve isoprene aerosol predictions (Ying et al., 2015). Changes in the SOA module included the surface uptake of dicarbonyls and isoprene epoxides, as well as predictions of glyoxal and methylglyoxal (Ying et al., 2015). The aerosol yields were updated to account for vapor wall loss during chamber experiments as described by Zhang et al. (2014). The S11 gas phase mechanism and the SOA module were
125 further expanded with a precursor tracking scheme to track emissions from different sources separately so that the formation of SOA could be determined. The complete description of SOA source tracking has been described by Zhang and Ying (2011) and Wang et al. (2018b), and a brief introduction is described below.



The modified S11 mechanism expands the specific original reactions into two sets of similar reactions to track the formation of O₃ and SOA. For the source apportionment of O₃, the amount of O₃ formed from NO_x and VOCs are determined and then they are apportioned to different sources, which are tracked using non-reactive O₃ tracers. In addition, the different sources of O₃ formed in the transition regime are also calculated similarly to NO_x and VOCs (Wang et al., 2019). As for SOA, the specific source X (for instance, biogenic source) is tracked by adding a superscript X on the precursors related to SOA (like TERP, the abbreviation of monoterpene in the S11 photochemical mechanism) and their products, while the contributions from all other sources are simulated based on none-tagged TERP. The tagged specie TERP^x reacts with OH to form the primary product TRPRXN^x, which is the counter species for aerosol precursor from monoterpenes and subsequently formed semi-volatile oxidation products SV_TRP1^x and SV_TRP2^x based on the two-product approach and thus determines the fine mode SOA species ATRP1^x and ATRP2^x due to gas-to-particle partitioning. By considering those species with the superscript X, it is possible to track the SOA formed by ATRP of source X. The contributions of other precursors of SOA are calculated using the same approach.

2.3 Model Application

The WRF model v3.6.1 was used to generate meteorological conditions for MEGAN and CMAQ. The modelling domain in WRF was 36 km × 36 km in horizontal spatial resolution, which covers China and its surrounding countries in East Asia (Fig. S1) (Zhang et al., 2012). The boundary and initial conditions applied in WRF were from the National Centers for Environmental Prediction (NCEP) Final (FNL) Operational Model Global Tropospheric Analyses dataset (available at <http://rda.ucar.edu/datasets/ds083.2/>, last access: 18 May 2022). The physical options used for the WRF model were presented in Table S1. The MEGANv2.1 was applied to estimate 19 compound classes of BVOCs (Guenther et al., 2012). In MEGAN, the LC and LAI datasets in 2016 were used and then were gridded to the same spatial resolution to generate PFTs fractions and LAIv maps as inputs for the model. The CMAQ model used a horizontal domain of 197 × 127 grid cells (Fig. 1) that covers China and its surrounding areas. The meteorological conditions as inputs to CMAQ model were provided by the WRF model v3.6.1. The anthropogenic emissions of China used the datasets from Multiresolution Emission Inventory for China (MEIC; available at <http://www.meicmodel.org>, last access: 3 May 2022), which was developed by Tsinghua University, and the Emissions Database for Global Atmospheric Research (EDGAR) v4.3 (available at http://edgar.jrc.ec.europa.eu/overview.php?v=_431, last access: 10 May 2022) was used as the anthropogenic emissions from other countries.

Table 1 presents the setup of the simulation scenarios. Scenarios C1 to C3 use MCD12Q1 as the PFTs input and different LAI inputs to investigate the effects of varied LAI datasets on BVOC emissions, while the impacts of different PFTs maps on BVOC estimations are studied in scenarios C1, C4, and C5, which use the GLASS as the LAI input. It should be noted that those experiments use the same meteorological conditions, which are provided by the WRF model, for BVOC estimations. Besides BVOC simulations, a one-year CMAQ simulation based on five cases is conducted for the year 2016 in China with the same meteorological conditions and anthropogenic emissions to investigate the impacts of BVOCs on O₃ and SOA concentrations.



3 Results and discussion

3.1 Model performance

165 Temperature (T2), relative humidity (RH), wind speed (WS) and wind direction (WD) at 10 m above the surface were compared to observations from the National Climate Data Center (NCDC, available at <https://www.ncei.noaa.gov/access>, last access: 13 May 2022). The statistical measures and results are shown in Table S3 and Table S4, respectively. T2 predictions are slightly lower than observations in the whole year with negative mean bias (MB) values slightly lower than the benchmarks suggested by Emery et al. (2001). Summer and fall show better performance than spring and winter. Although the gross error (GE) values of WS are within the criteria of 2 in all seasons, the WRF model still overpredicted the WS. The MB values of WD meet the benchmarks of ± 10 in all seasons, but the GE values are over the benchmarks of ± 30 . In spring and winter, the predicted RH is slightly lower than the observations, while it is overestimated in summer and fall. The model successfully captures the day-to-day variations of temperature in most cities in China (Fig. S2). The performance of the WRF model in this study is comparable to previous studies (Hu et al., 2016; Wang et al., 2018a; Wang et al., 2010; Ma et al., 2021). Generally, the meteorological conditions predicted by the WRF model are acceptable as inputs for the CMAQ model in follow-up research.

175 Hourly observations from the publishing website of the China National Environmental Monitoring Center (available at <http://www.cnemc.cn/>, last access: 4 May 2022) were used to validate the CMAQ model prediction of O₃ and PM_{2.5}. In order to investigate the impacts of varied total BVOC emissions on main air pollutants, the model performance was evaluated separately for different cases. Table S5 presents the model performance statistics of air pollutants, including maximum daily averaged 1h (MDA1) O₃, maximum daily averaged 8h (MDA8) O₃. The evaluated statistics of mean observations (OBS), mean predictions (PRE), mean fractional bias (MFB), mean fractional error (MFE), mean normalized bias (MNB), and mean normalized error (MNE) were calculated for each case in 2016. Cut-off concentrations of 60 ppb were used for both MDA1 O₃ and MDA8 O₃ in this validation, respectively, which were suggested by the US EPA (EPA, 2005). In general, the model performance on MDA1 O₃ and MDA8 O₃ in all cases in China and its important regions meet the model performance benchmarks suggested by EPA (2005), although the model still overestimates the O₃ concentrations. In China, the MNB value of MDA1 O₃ ranges from 0.02~0.05 and the MNE value of MDA1 O₃ ranges from 0.18~0.19, which are within the criteria of ± 0.15 and ± 0.3 , respectively. In important regions, the MDA1 O₃ concentration in the PRD shows a better consistency with the observations than in the YRD and NCP. The statistical values of MDA1 O₃ in C4 are closer to benchmarks than in the other cases, indicating the better performance of the model simulation of C4. In addition to the comparison of MDA1 O₃, the MNB values of MDA8 O₃ are slightly higher than those of MDA1 O₃, and they also meet the criteria. The MDA8 O₃ in C4 shows better agreement with observations because the statistics are closer to the criteria.

Table S6 presents the model performance statistics on PM_{2.5}. The statistical values of PM_{2.5} in all cases are within the criteria (MFB $\leq \pm 60$ % and MFE ≤ 75 %) suggested by Boylan and Russell (2006). However, the predicted PM_{2.5} is slightly lower



195 than the observations, which can be indicated by the negative MFB values. In important regions, the MNB values in the YRD
are slightly higher than in other regions, while MFE and MNE values are higher in the PRD. Compared to other cases, the
statistical values of $PM_{2.5}$ in C4 are lower, indicating a better performance of $PM_{2.5}$ in C4. Therefore, the BVOC emissions in
C4 generated by using C3S LC and GLASS are the best BVOC inventory in this study. Besides, although C1, C2, and C3
adopt LAI satellite products with different accuracies, results show the similar model performance of them, suggesting that the
accuracy of LAI satellite products does not correlate with the BVOC estimations and the performance of air quality. The
200 overall statistical values meet the criteria in all cases, which indicates that the O_3 and $PM_{2.5}$ are well captured by the model.
Generally, the simulation results of air pollutants in this study are acceptable for the source apportionment study of O_3 and
SOA, which was comparable to other studies (Hu et al., 2016; Wu et al., 2020; Liu et al., 2020).

3.2 Simulated BVOC emissions in China

3.2.1 Quantity of BVOC emissions

205 Table 3 shows the total amount of BVOC emissions and its major components of each case in China in 2016. In general, the
LC satellite products show a relatively higher impact on BVOC emissions than LAI satellite products. Isoprene accounts for
the largest share of BVOC emissions with an average of 54% for all cases, and the difference in the isoprene emission of each
case is the main reason resulting in the discrepancy in total BVOC emissions between each case. C5 shows the highest BVOC
emissions of 37.39 Tg with the isoprene emission of 22.73 Tg, which is also the highest of all cases. In contrast, BVOC
210 emissions of 25.42 Tg and the isoprene emission of 12.1 Tg in C4 both are the lowest in all cases. The emissions of BVOC
species in C1 are similar to those of C3, and the relative difference in total BVOC emissions between them is less than 1%.
This may be because the LAIv values in western China in C3 are higher than that of C1, while those in eastern China are lower
than that of C1, and the combination of the two parts makes the BVOC emissions of C3 and C1 close (Fig. S3). The MOD15
LAI dataset used in C2 shows significant differences from C1, with the variance values of LAIv that can reach ~ 2.0 in most
215 areas of China, and the discrepancy results in the remarkable difference in isoprene between the two cases. In addition to the
impact of LAI datasets on BVOC emissions, the LC dataset used in C4 leads to a 21.4% decrease in the isoprene emission
compared to C1, while C5 with the CGLS LC dataset results in an 8% increase in the isoprene emission, which is due to the
higher percentage broadleaf tree cover in CGLS LC products (Fig. S4 and Table 2). Although the total BVOC emissions in C5
are 1.29 Tg higher than those in C1, the emissions of monoterpenes, sesquiterpenes, and other VOCs are lower than in C1.
220 This is possibly induced by the discrepancy in the distribution of shrubs and grass between C1 and C5 (Fig. S4).

3.2.2 Temporal and spatial variation of BVOC emissions

Figure 3 presents the seasonal variations in isoprene, monoterpenes, sesquiterpenes, and total BVOC emissions in all cases in
China. In general, using different LAI and LC products does have an impact on the temporal variability in the BVOC emissions.



225 The BVOC emissions have a similar seasonal change trend in all cases due to the temperature, solar radiation, and vegetation
covers rising and then falling as season transit. Such variation results in BVOC emissions being concentrated in summer,
accounting for 60.9%~63.8% of total BVOC emissions, while winter BVOC emissions contribute only 2.9%~3.4% of total
emissions. The isoprene emission is the biggest contributor to BVOCs and contributions can reach 7.94~14.79 Tg in summer
in all cases. The percentage of winter monoterpenes in the total monoterpenes is higher than that of isoprene and sesquiterpenes,
230 indicating that isoprene and sesquiterpenes are more sensitive than monoterpenes to temperature changes. The reason can
attribute to the higher temperature coefficients of sesquiterpenes compared to those of monoterpenes (Helmig et al., 2006). C4
used the C3S LC and GLASS shows the lowest emissions in total BVOCs and its main species among each season. The
monoterpene emissions show little sensitivity to LAI changes between C1, C2, and C3 in summer compared to isoprene and
sesquiterpene emissions. In contrast, variations in different LC datasets have a higher impact on the monoterpene emissions
235 and total BVOC emissions in summer. Furthermore, the isoprene emission of C5 is the highest among the cases, but the
monoterpene and sesquiterpene emissions in C5 are lower than that in C3 as well as in C1, which may be due to the higher
distribution of broadleaf trees with the high isoprene EF and lower distribution of grass with the high monoterpene and
sesquiterpene EF in CGLS LC compared to those in MCD12Q1. The differences in BVOC emissions between C1 and the
other cases are larger when the temperature rises, reaching the maximum in summer, which is because that BVOC emissions
240 are susceptible to the influence of temperature and radiation in the atmosphere (Guenther et al., 2006;Guenther et al., 2012).

Since a large proportion of BVOCs is released in summer, which contributes about 62% of total annual emissions, the analysis
of the spatial distribution is mainly concentrated on summer BVOC emissions. Figure 4 illustrates the spatial distribution of
total BVOCs, isoprene, monoterpenes, and sesquiterpenes during summer in C1 as well as the comparisons between C1 and
245 the other cases. In general, the difference in spatial distribution of BVOCs mainly focuses on central and southeastern China,
and the differences induced by different LC products are more significant than by different LAI products. The isoprene,
monoterpenes, and sesquiterpenes emissions show similar distribution patterns with hotspots primarily located in the central
and southeastern China for all cases, as shown in Fig. 4 (panels f, k and p). This is due to the high density of tree covers in
those regions. Although the GLASS has the same temporal resolution of 8 days as MOD15, differences between the two
250 products still play an important role in impacting the BVOC emissions (Fig. 2 and Fig. 4b). According to Fig. 4 (panels a and
q), the difference of emission distribution of isoprene and sesquiterpene between the C1 and C2 is generally consistent with
the difference in GLASS and MOD15 in summer. Similar effects are occurred between the LAI datasets of GLASS and CGLS
in C1 as well as C3 (Fig. 4h and r), which indicates that the isoprene and sesquiterpene emissions have the same variation
trend when using the different LAI inputs. The changes in the spatial distribution of BVOC emissions in C4 and C5 are more
255 significant compared to C2 and C3. The higher emissions of three main BVOC species in the south of China in C1 than in C4
are due to the higher vegetation cover in C1, as shown in Fig. 4 (panels i, n and s). C4 used the C3S LC as the model inputs
with crops dominating nearly half of China, and the relatively low EF of the crop for three main BVOC species compared to
the other PFTs, resulting in the lower BVOC estimations in C4 (Fig. 1 and Fig. S3). The spatial distribution of isoprene



emission in C5 is conspicuously different than in C1, which is consistent with a difference in the broadleaf tree distribution in
260 the inputs (Fig. S3). Even though C5 shows a higher forest cover than C1 in the north of China, the isoprene emission in C1 is
higher than C5 in that place, which is likely due to the difference in the grass distribution and the impact of temperature. Cooler
temperatures at higher latitudes inhibit the release of isoprene from forests (Guenther et al., 2006).

3.2.3 Comparison with previous studies

Table 4 illustrates the annual BVOC emissions estimated by MEGAN in China in this study and previous studies. The annual
265 BVOC emissions in this study range from 25.42 ~ 37.39 Tg, which is within the range of 17.30 ~ 54.60 Tg from 2001 to 2018
published in the literatures. BVOC emissions estimated by this study are higher than 18.85 and 23.54 Tg estimated by Fu and
Liao (2012), and Wu et al. (2020), respectively. However, results in this study are lower than the 42.5 Tg for 2003 estimated
by Li et al. (2013) , and 54.6 Tg estimated by Li et al. (2020). The differences between this study with previous studies can be
induced by many factors. The increase in forest coverages may be the main reason for the large difference. According to the
270 reports in National Forest Resources Census, the forest coverages increased relatively about 18.8% from 2003 to 2013 (FGA,
2006, 2014). In addition, the MEGAN inputs as well as algorithms in the model will have an impact on the simulation of
BVOC emissions. In this study, the default EFs listed in Guenther et al. (2012) are used for all BVOC species. Fu and Liao
(2012) used a set of EFs with 25 PFTs for isoprene and monoterpenes, which are generally lower than the default EFs for
MEGAN, leading to much lower BVOC emissions of 18.85 Tg than in this study. Although the same datasets of MODIS
275 MOD15A2H and MODIS MCD12Q1 were used as LAI and PFTs inputs for MEGAN, the estimate in Wu et al. (2020) is
lower than in this study due to lower area fractions of the broadleaf tree, which has the highest isoprene EF than other PFTs
(Guenther et al., 2012), and absent of area fraction of crop when calculating BVOC emissions for China. There is a considerable
difference in BVOC emissions between this study and those of Li et al. (2013). The difference is mainly due to the combined
effect of PFTs and algorithms. Li et al. (2013) developed a new vegetation classification based on four different plant statistics
280 for China with 82 PFTs, and used different algorithms to calculate the leaf biomass for different plants. Besides, the
overestimated temperature in Wang et al. (2021) may be the main reason resulting in a higher estimate of 35.48 Tg for 2016
than in our study. In conclusion, uncertainties in the MEGAN simulations can be attributed to these factors in different years,
and these uncertainties can lead to significant differences between this study and previous studies. Therefore, the simulated
BVOC emissions are within acceptable limits compared to the previous studies.

285 3.3 Sensitivity of O₃ to BVOC emissions

3.3.1 Spatial distribution of O₃

Figure 5 displays the spatial distribution of MDA1 O₃ and MDA8 O₃ concentration formed by the BVOCs during the summer
in C1 as well as the difference between C1 and the other cases. The differences in emissions of BVOCs between C1 and other
cases have impacts on the spatial distribution of O₃, and the impacts from changing LC inputs are greater than that from



290 changing LAI inputs. The O₃ concentration hotspots are mainly concentrated in central and eastern China, where MDA1 O₃
concentrations can reach more than 12 ppb in C1. This is possibly due to the effect of Asian summer monsoon, which brings
in oceanic air masses with low O₃ concentrations and transports O₃ from southern to central and northern China (Zhao et al.,
2010; Li et al., 2018). As shown in Fig. 5d, the spatial distribution of O₃ concentration in C4 is conspicuously different than in
C1, especially in central and eastern China, where the differences are up to 4.8-6.9 ppb. In addition, higher BVOC emissions
295 in C5 than in C1 do not have a significant impact on O₃ formation in southern China (Fig. 4), which is possibly due to the
effect of O₃-NO_x-VOC sensitivity. According to the study of Jin and Holloway (2015), these regions belong to NO_x-limited
regions, in which NO_x is limited but VOCs are abundant, and thus the higher BVOC emissions have few impacts on the
formation of O₃. In contrast, the areas with low VOCs emissions will contribute more to the O₃ formation when VOCs
emissions increase, such as the NCP and YRD. MDA8 O₃ shows a similar spatial distribution pattern to MDA1 O₃ in C1, but
300 the concentration is 3-6 ppb lower than that of MDA1 O₃.

3.3.2 Temporal distribution of O₃

Figure 6 illustrates the contribution of BVOC emissions to MDA1 O₃ and MDA8 O₃ in important regions and China in different
seasons. In general, the differences of O₃ concentration between each case show seasonal variations in China and are significant
in summer. O₃ concentrations formed by the biogenic source are high in summer and low in winter, which is due to the
305 combined effect of BVOC emissions and wind. The summer monsoon transports a large amount of O₃ from southern China to
the YRD and NCP (Zhao et al., 2010), resulting in a large difference in O₃ concentrations between different cases. C1, C3, and
C5 have a similar O₃ concentration in each season due to the similar BVOC emissions. The highest MDA1 O₃ of 8.2 ppb is
shown in C1 in the YRD, while the lowest value of 4.6 ppb is observed in C4, which is due to the effect of O₃-NO_x-VOC
sensitivity. Higher BVOC emissions in VOC-limited regions lead to the higher O₃ formation (Jin and Holloway, 2015). In
310 most areas of China, especially in the YRD and NCP, the discrepancies between each case are expanded with the increase of
the biogenic O₃ concentration, which indicates that seasonal variations of BVOC emissions have an impact on the differences
between each case. Besides, the wind effect also plays an important role in seasonal variations of O₃ concentrations (Fig. S5),
especially in the PRD. The clean oceanic air masses are brought by the wind to the southeast of China resulting in a decrease
in local O₃ concentrations (Zhao et al., 2010). However, the wind in fall transports heavy pollutants from northern to southern
315 China, increasing the O₃ concentrations in southern China (Li et al., 2018). Therefore, the seasonal variations of O₃ and
differences in O₃ concentrations between each case are not significant in the PRD due to the combine effect of wind and
temperature (Table S7). In all cases, MDA8 O₃ shows a similar temporal distribution to MDA1 O₃ in China and important
regions, but the fall contribution is lower than the spring contribution, which is the opposite of MDA1 O₃.



3.4 Sensitivity of SOA to BVOC emissions

320 3.4.1 Spatial distribution of SOA and components

Figure 7 presents the spatial distribution of BSOA during the summer in C1 as well as the difference between C1 and other cases. In general, using different LC datasets as MEGAN inputs shows more significant impacts on SOA formation. The hotspots of BSOA are mainly concentrated in central and eastern China, especially Sichuan basin, where the BSOA concentration is up to $12 \mu\text{g m}^{-3}$. This is because that the high surface wind brings the BSOA from southern China to central
325 China and then, low wind speeds and the topography condition in Sichuan basin, which are against the pollutant diffusion, result in accumulation of BSOA (Li et al., 2017). The differences in BSOA concentrations between C1 and C2 are inconspicuous, even though the differences in total BVOC emissions between them exceed 5 Tg, indicating that the LAI inputs have few impacts on the BSOA concentrations. In contrast, the LC inputs show higher impacts on BSOA concentrations. According to Fig. 7d, the difference in the BSOA concentration between C1 and C4 is conspicuous in central China, especially
330 in regions with high BSOA concentrations, such as Sichuan, Hunan, and Hubei provinces, where the differences are up to 5.3-8.4 $\mu\text{g m}^{-3}$. The spatial distribution of BSOA differences between C1 and C5 is similar to the spatial distribution of isoprene emission differences between them, suggesting that BSOA concentrations are more sensitive to isoprene emission than monoterpenes and sesquiterpenes. Considering the share of BSOA in the total SOA concentration in summer, the difference in BVOC emissions due to changing the inputs to the MEGAN model can therefore have a significant impact on SOA
335 concentrations estimated by CMAQ.

Figure 8 displays the spatial distribution of SOA formed by isoprene (ISOA), monoterpenes (MSOA) and sesquiterpenes (SSOA) during summer in C1 as well as the difference between C1 and the other cases. The ISOA, MSOA and SSOA show a similar spatial distribution for all cases in China. According to Fig. 8 (panels a, b and c), the high SOA concentration from
340 these three BVOC species mainly concentrated in central and eastern China. This phenomenon is likely due to the combined effect of BVOC emissions and meteorological conditions in these areas. A large amount of SOA is generated in southern China and then transported to central and eastern China due to wind effects in summer. The ISOA concentrations are 1 time higher than MSOA and 1.5 times higher than SSOA due to the higher isoprene emission, indicating that the isoprene is the most important contributor to the SOA in the biogenic source during the summer. Furthermore, the sesquiterpene emissions are also
345 a significant contributor to the formation of SOA even with a lower emission rate compared to isoprene and monoterpenes. Comparing C1 with other cases, the difference in the ISOA concentration basically shows a certain correlation with the difference in BVOCs (Fig. 4). If the spatial distribution of the isoprene emission from C1 is higher than in the other case, then this is the same for the spatial distribution of ISOA concentrations, and vice versa. This fact also acts on MSOA and SSOA. Moreover, the difference in ISOA concentrations between C1 and C4 is higher than that in MSOA and SSOA, which can
350 attribute to the large discrepancy in their isoprene emission (Fig. 8j, k, and l). The ISOA concentrations in southeastern China are lower in C1 than in C5, but the MSOA and SSOA concentrations are higher than in C5, which is due to the difference in



BVOC estimations between them. Since isoprene contributes most to the BVOCs compared to monoterpenes and sesquiterpenes, modifying the input of MEGAN tends to have a large impact on the isoprene emission. Therefore, the difference in BVOC emissions induced by different MEGAN inputs, especially isoprene, do have an impact on the formation of SOA. The magnitude of this effect depends on the amount of difference in BVOC emissions.

3.4.2 Temporal distribution of SOA

Figure 9 illustrates the seasonal variation in biogenic SOA (BSOA) concentrations in China and the important regions for all cases. In general, the differences in BSOA concentrations between each case are more significant in summer than in other seasons. The BSOA concentration follows the temporal trend of summer > spring > fall > winter in China, NCP as well as YRD. However, the higher BSOA concentration in the PRD occurs in spring, which is due to changes in the wind direction from the erratic wind in spring to the southerly wind in summer (Fig. S6). There are slight differences in BSOA concentrations between C1, C3 and C5 in China, while the differences in C2 and C4 are more conspicuous, especially in the YRD, in which the summer BSOA in C1 is 2.5 times higher than that in C4. The BSOA in C1 is higher than C5 in most areas of China except for the PRD, which is due to the higher isoprene emission in C5 in the PRD (Fig. 4).

4 Conclusion

In this study, we used the different LC datasets as the MEGAN inputs to estimate the BVOC emissions in 2016 over China and then utilized the WRF-CMAQ model to quantify the contribution of BVOCs to O₃ and SOA concentrations. Besides, the impact induced by changing LC on O₃ and SOA formation was also evaluated. Five experiments were conducted based on three LAI satellite products (GLASS, MOD15, and CGLS) and three LC satellite products (MCD12Q1, C3S, and CGLS). According to model validations, C4 with GLASS and C3S LC was the better choice for China BVOC estimations compared to other scenarios. BVOC emissions in China ranged from 25.42 to 37.39 Tg in 2016 and were mainly concentrated in central and southeastern China, which was due to the high density of tree covers in those regions. In comparison with LAI inputs, using different LC satellite products had a more significant impact on BVOC emissions.

The high O₃ and BSOA concentrations formed by the biogenic source mainly concentrated in central and eastern China in summer, especially in Sichuan basin. This was because that the high surface wind brings the O₃ and BSOA from southern to central China and then, low wind speeds and the topography condition in Sichuan basin, which are against the pollutant diffusion, resulting in the accumulation of air pollutants. In addition, the high NO_x emission regions such as the NCP and YRD contributed more to the O₃ formation when there were enough VOCs. According to dataset comparisons, C1 showed the highest concentrations of O₃ and BSOA formed by BVOCs, especially in the YRD, while the lowest values occurred in C4. Changing LC datasets for the model input has more conspicuous impacts on O₃ and SOA formation.

From 2000 to 2017, global leaf area of vegetation increased by 6.6% due to the direct land-use management, which may also enhance BVOC emissions, leading to further effects on air quality. Thus, the findings of this study can be extended to other



regions and global scales, suggesting an urgent need to construct a reliable BVOC emission inventory for local and global scales, and evaluate their impacts on air quality. However, the limitation of observed data of BVOCs and organic components impedes the construction of the accurate emission inventory. Therefore, field measurements are needed to provide more data for model validations. In addition, urban BVOC emissions play important roles in urban air quality, it would be interesting to study the impact of biogenic sources on the urban air quality by using high resolution LC satellite maps.

Author contributions. JM conducted the modelling and write the paper. SZ and SW assisted with data analysis. PW and HZ designed the study, discussed the results, and edited the paper.

Competing interests. The authors declare that they have no conflict of interest.

Financial support. The DFG-NSFC Sino-German AirChanges project (448720203), National Natural Science Foundation of China (42077194/42061134008), and Shanghai International Science and Technology Partnership Project (No. 21230780200) funded this work.

References

- Boylan, J. W., and Russell, A. G.: PM and light extinction model performance metrics, goals, and criteria for three-dimensional air quality models, *Atmos. Environ.*, 40, 4946-4959, <https://doi.org/10.1016/j.atmosenv.2005.09.087>, 2006.
- Buchhorn, M., Smets, B., Bertels, L., DeRoo, B., Lesiv, M., Tsendbazar, N.-E., Herold, M., and Fritz, S.: Copernicus Global Land Service: Land Cover 100m: collection 3: epoch 2019: Globe (V3.0.1) [Data set], Zenodo, <https://doi.org/10.5281/zenodo.3939050>, 2020.
- Byun, D., and Schere, K. L.: Review of the Governing Equations, Computational Algorithms, and Other Components of the Models-3 Community Multiscale Air Quality (CMAQ) Modeling System, *Appl. Mech. Rev.*, 59, 51-77, 10.1115/1.2128636, 2006.
- C3S: Product User Guide and Specification, 2021.
- Calfapietra, C., Fares, S., Manes, F., Morani, A., Sgrigna, G., and Loreto, F.: Role of Biogenic Volatile Organic Compounds (BVOC) emitted by urban trees on ozone concentration in cities: A review, *Environ. Pollut.*, 183, 71-80, 10.1016/j.envpol.2013.03.012, 2013.
- Carlton, A. G., and Baker, K. R.: Photochemical Modeling of the Ozark Isoprene Volcano: MEGAN, BEIS, and Their Impacts on Air Quality Predictions, *Environ. Sci. Technol.*, 45, 4438-4445, 10.1021/es200050x, 2011.
- Carter, W. P. L., and Heo, G.: Development of revised SAPRC aromatics mechanisms, *Atmos. Environ.*, 77, 404-414, <https://doi.org/10.1016/j.atmosenv.2013.05.021>, 2013.
- Emery, C., Tai, E., and Yarwood, G.: Enhanced meteorological modeling and performance evaluation for two texas episodes, Report to the Texas Natural Resources Conservation Commission, prepared by ENVIRON, International Corp., Novato, CA, 2001.
- Emmerson, K. M., Cope, M. E., Galbally, I. E., Lee, S., and Nelson, P. F.: Isoprene and monoterpene emissions in south-east Australia: comparison of a multi-layer canopy model with MEGAN and with atmospheric observations, *Atmos. Chem. Phys.*, 18, 7539-7556, 10.5194/acp-18-7539-2018, 2018.
- EPA, U. S.: Guidance on the Use of Models and Other Analyses in Attainment Demonstrations for the 8-hour Ozone NAAQS, EPA-454/R-05-002, 2005.
- Fehsenfeld, F., Calvert, J., Fall, R., Goldan, P., Guenther, A. B., Hewitt, C. N., Lamb, B., Liu, S., Trainer, M., Westberg, H., and Zimmerman, P.: Emissions of volatile organic compounds from vegetation and the implications for atmospheric chemistry, *Global Biogeochem Cycles.*, 6, 389-430, <https://doi.org/10.1029/92GB02125>, 1992.
- The Sixth National Forest Resources Inventory: <http://www.forestry.gov.cn/portal/main/s/65/content-90.html>, 2006.
- FGA, C.: The Eighth National Forest Resources Inventory, 2014.
- Friedl, M., and Sulla-Menashe, D.: MCD12Q1 MODIS/Terra+Aqua Land Cover Type Yearly L3 Global 500m SIN Grid V006 [Data set], NASA EOSDIS Land Processes DAAC, <https://doi.org/10.5067/MODIS/MCD12Q1.006>, 2019.



- Fu, Y., and Liao, H.: Simulation of the interannual variations of biogenic emissions of volatile organic compounds in China: Impacts on tropospheric ozone and secondary organic aerosol, *Atmos. Environ.*, 59, 170-185, <https://doi.org/10.1016/j.atmosenv.2012.05.053>, 2012.
- 425 Fu, Y., and Liao, H.: Impacts of land use and land cover changes on biogenic emissions of volatile organic compounds in China from the late 1980s to the mid-2000s: implications for tropospheric ozone and secondary organic aerosol, *Tellus B.*, 66, 10.3402/tellusb.v66.24987, 2014.
- Fuster, B., Sánchez-Zapero, J., Camacho, F., García-Santos, V., Verger, A., Lacaze, R., Weiss, M., Baret, F., and Smets, B.: Quality Assessment of PROBA-V LAI, fAPAR and fCOVER Collection 300 m Products of Copernicus Global Land Service, *Remote Sens.*, 12, 10.3390/rs12061017, 2020.
- 430 Guenther, A., Hewitt, C. N., Erickson, D., Fall, R., Geron, C., Graedel, T., Harley, P., Klinger, L., Lerdau, M., McKay, W. A., Pierce, T., Scholes, B., Steinbrecher, R., Tallamraju, R., Taylor, J., and Zimmerman, P.: A global model of natural volatile organic compound emissions, *J. Geophys. Res. Atmos.*, 100, 8873-8892, <https://doi.org/10.1029/94JD02950>, 1995.
- Guenther, A., Karl, T., Harley, P., Wiedinmyer, C., Palmer, P. I., and Geron, C.: Estimates of global terrestrial isoprene emissions using MEGAN (Model of Emissions of Gases and Aerosols from Nature), *Atmos. Chem. Phys.*, 6, 3181-3210, 10.5194/acp-6-3181-2006, 2006.
- 435 Guenther, A. B., Jiang, X., Heald, C. L., Sakulyanontvittaya, T., Duhl, T., Emmons, L. K., and Wang, X.: The Model of Emissions of Gases and Aerosols from Nature version 2.1 (MEGAN2.1): an extended and updated framework for modeling biogenic emissions, *Geosci. Model Dev.*, 5, 1471-1492, 10.5194/gmd-5-1471-2012, 2012.
- Helmig, D., Ortega, J., Guenther, A., Herrick, J. D., and Geron, C.: Sesquiterpene emissions from loblolly pine and their potential contribution to biogenic aerosol formation in the Southeastern US, *Atmos. Environ.*, 40, 4150-4157, <https://doi.org/10.1016/j.atmosenv.2006.02.035>, 2006.
- 440 Hu, J., Chen, J., Ying, Q., and Zhang, H.: One-year simulation of ozone and particulate matter in China using WRF/CMAQ modeling system, *Atmos. Chem. Phys.*, 16, 10333-10350, 10.5194/acp-16-10333-2016, 2016.
- Jiang, J., Aksoyoglu, S., Ciarelli, G., Oikonomakis, E., El-Haddad, I., Canonaco, F., O'Dowd, C., Ovadnevaite, J., Cruz Minguillon, M., Baltensperger, U., and Prevot, A. S. H.: Effects of two different biogenic emission models on modelled ozone and aerosol concentrations in Europe, *Atmos. Chem. Phys.*, 19, 3747-3768, 10.5194/acp-19-3747-2019, 2019a.
- 445 Jiang, J. H., Aksoyoglu, S., Ciarelli, G., Oikonomakis, E., El-Haddad, I., Canonaco, F., O'Dowd, C., Ovadnevaite, J., Minguillon, M. C., Baltensperger, U., and Prevot, A. S. H.: Effects of two different biogenic emission models on modelled ozone and aerosol concentrations in Europe, *Atmos. Chem. Phys.*, 19, 3747-3768, 10.5194/acp-19-3747-2019, 2019b.
- 450 Jin, X., and Holloway, T.: Spatial and temporal variability of ozone sensitivity over China observed from the Ozone Monitoring Instrument, *J. Geophys. Res. Atmos.*, 120, 7229-7246, <https://doi.org/10.1002/2015JD023250>, 2015.
- Kim, H. K., Woo, J. H., Park, R. S., Song, C. H., Kim, J. H., Ban, S. J., and Park, J. H.: Impacts of different plant functional types on ambient ozone predictions in the Seoul Metropolitan Areas (SMAs), Korea, *Atmos. Chem. Phys.*, 14, 7461-7484, 10.5194/acp-14-7461-2014, 2014.
- Laothawornkitkul, J., Taylor, J. E., Paul, N. D., and Hewitt, C. N.: Biogenic Volatile Organic Compounds in the Earth System, *New Phytol.*, 183, 27-51, 2009.
- 455 Leung, D. Y. C., Wong, P., Cheung, B. K. H., and Guenther, A.: Improved land cover and emission factors for modeling biogenic volatile organic compounds emissions from Hong Kong, *Atmos. Environ.*, 44, 1456-1468, 10.1016/j.atmosenv.2010.01.012, 2010.
- Li, J., Zhang, M., Wu, F., Sun, Y., and Tang, G.: Assessment of the impacts of aromatic VOC emissions and yields of SOA on SOA concentrations with the air quality model RAMS-CMAQ, *Atmos. Environ.*, 158, 105-115, <https://doi.org/10.1016/j.atmosenv.2017.03.035>, 2017.
- 460 Li, L., Yang, W., Xie, S., and Wu, Y.: Estimations and uncertainty of biogenic volatile organic compound emission inventory in China for 2008–2018, *Sci. Total. Environ.*, 733, 139301, <https://doi.org/10.1016/j.scitotenv.2020.139301>, 2020.
- Li, L. Y., Chen, Y., and Xie, S. D.: Spatio-temporal variation of biogenic volatile organic compounds emissions in China, *Environ. Pollut.*, 182, 157-168, <https://doi.org/10.1016/j.envpol.2013.06.042>, 2013.
- 465 Li, S., Wang, T., Huang, X., Pu, X., Li, M., Chen, P., Yang, X.-Q., and Wang, M.: Impact of East Asian Summer Monsoon on Surface Ozone Pattern in China, *J. Geophys. Res. Atmos.*, 123, 1401-1411, <https://doi.org/10.1002/2017JD027190>, 2018.
- Liu, J., Shen, J., Cheng, Z., Wang, P., Ying, Q., Zhao, Q., Zhang, Y., Zhao, Y., and Fu, Q.: Source apportionment and regional transport of anthropogenic secondary organic aerosol during winter pollution periods in the Yangtze River Delta, China, *Sci. Total. Environ.*, 710, 135620, <https://doi.org/10.1016/j.scitotenv.2019.135620>, 2020.
- 470 Ma, J., Shen, J., Wang, P., Zhu, S., Wang, Y., Wang, P., Wang, G., Chen, J., and Zhang, H.: Modeled changes in source contributions of particulate matter during the COVID-19 pandemic in the Yangtze River Delta, China, *Atmos. Chem. Phys.*, 21, 7343-7355, 10.5194/acp-21-7343-2021, 2021.
- Messina, P., Lathièrre, J., Sindelarova, K., Vuichard, N., Granier, C., Ghattas, J., Cozic, A., and Hauglustaine, D. A.: Global biogenic volatile organic compound emissions in the ORCHIDEE and MEGAN models and sensitivity to key parameters, *Atmos. Chem. Phys.*, 16, 14169-14202, 10.5194/acp-16-14169-2016, 2016.
- 475 Myneni, R. B., Knyazikhin, Y., and Park, T.: MOD15A2H MODIS/Terra Leaf Area Index/FPAR 8-Day L4 Global 500m SIN Grid V006 [Data set], NASA EOSDIS Land Processes DAAC, <https://doi.org/10.5067/MODIS/MOD15A2H.006>, 2015.
- NFGA: China Forest Resources Report (2014-2018), 1 ed., China Forestry Press, 2019.



- 480 Opacka, B., Muller, J.-F., Stavrakou, T., Bauwens, M., Sindelarova, K., Markova, J., and Guenther, A. B.: Global and regional impacts of land cover changes on isoprene emissions derived from spaceborne data and the MEGAN model, *Atmos. Chem. Phys.*, 21, 8413-8436, 10.5194/acp-21-8413-2021, 2021.
- Pfister, G. G., Emmons, L. K., Hess, P. G., Lamarque, J. F., Orlando, J. J., Walters, S., Guenther, A., Palmer, P. I., and Lawrence, P. J.: Contribution of isoprene to chemical budgets: A model tracer study with the NCAR CTM MOZART-4, *J. Geophys. Res. Atmos.*, 113, <https://doi.org/10.1029/2007JD008948>, 2008.
- 485 Qin, M., Wang, X., Hu, Y., Ding, X., Song, Y., Li, M., Vasilakos, P., Nenes, A., and Russell, A. G.: Simulating Biogenic Secondary Organic Aerosol During Summertime in China, *J. Geophys. Res. Atmos.*, 123, 1100-1111, <https://doi.org/10.1029/2018JD029185>, 2018.
- Sindelarova, K., Granier, C., Bouarar, I., Guenther, A., Tilmes, S., Stavrakou, T., Muller, J. F., Kuhn, U., Stefani, P., and Knorr, W.: Global data set of biogenic VOC emissions calculated by the MEGAN model over the last 30 years, *Atmos. Chem. Phys.*, 14, 9317-9341, 10.5194/acp-14-9317-2014, 2014.
- 490 Situ, S., Guenther, A., Wang, X., Jiang, X., Turnipseed, A., Wu, Z., Bai, J., and Wang, X.: Impacts of seasonal and regional variability in biogenic VOC emissions on surface ozone in the Pearl River delta region, China, *Atmos. Chem. Phys.*, 13, 11803-11817, 10.5194/acp-13-11803-2013, 2013.
- Situ, S., Wang, X., Guenther, A., Zhang, Y., Wang, X., Huang, M., Fan, Q., and Xiong, Z.: Uncertainties of isoprene emissions in the MEGAN model estimated for a coniferous and broad-leaved mixed forest in Southern China, *Atmos. Environ.*, 98, 105-110, <https://doi.org/10.1016/j.atmosenv.2014.08.023>, 2014.
- 495 Stavrakou, T., Müller, J. F., Bauwens, M., De Smedt, I., Van Roozendaal, M., Guenther, A., Wild, M., and Xia, X.: Isoprene emissions over Asia 1979-2012: impact of climate and land-use changes, *Atmos. Chem. Phys.*, 14, 4587-4605, 10.5194/acp-14-4587-2014, 2014.
- Unger, N.: On the role of plant volatiles in anthropogenic global climate change, *Geophys. Res. Lett.*, 41, 8563-8569, 10.1002/2014GL061616, 2014a.
- 500 Unger, N.: Human land-use-driven reduction of forest volatiles cools global climate, *Nat. Clim. Change*, 4, 907-910, 10.1038/nclimate2347, 2014b.
- Volkamer, R., Jimenez, J. L., San Martini, F., Dzepina, K., Zhang, Q., Salcedo, D., Molina, L. T., Worsnop, D. R., and Molina, M. J.: Secondary organic aerosol formation from anthropogenic air pollution: Rapid and higher than expected, *Geophys. Res. Lett.*, 33, 10.1029/2006GL026899, 2006.
- 505 Wang, H., Wu, Q., Liu, H., Wang, Y., Cheng, H., Wang, R., Wang, L., Xiao, H., and Yang, X.: Sensitivity of biogenic volatile organic compound emissions to leaf area index and land cover in Beijing, *Atmos. Chem. Phys.*, 18, 9583-9596, 10.5194/acp-18-9583-2018, 2018a.
- Wang, H., Wu, Q., Guenther, A. B., Yang, X., Wang, L., Xiao, T., Li, J., Feng, J., Xu, Q., and Cheng, H.: A long-term estimation of biogenic volatile organic compound (BVOC) emission in China from 2001–2016: the roles of land cover change and climate variability, *Atmos. Chem. Phys.*, 21, 4825-4848, 10.5194/acp-21-4825-2021, 2021.
- 510 Wang, L., Jang, C., Zhang, Y., Wang, K., Zhang, Q., Streets, D., Fu, J., Lei, Y., Schreifels, J., He, K., Hao, J., Lam, Y.-F., Lin, J., Meskhidze, N., Voorhees, S., Evaris, D., and Phillips, S.: Assessment of air quality benefits from national air pollution control policies in China. Part I: Background, emission scenarios and evaluation of meteorological predictions, *Atmos. Environ.*, 44, 3442-3448, <https://doi.org/10.1016/j.atmosenv.2010.05.051>, 2010.
- Wang, P., Ying, Q., Zhang, H., Hu, J., Lin, Y., and Mao, H.: Source apportionment of secondary organic aerosol in China using a regional source-oriented chemical transport model and two emission inventories, *Environ. Pollut.*, 237, 756-766, <https://doi.org/10.1016/j.envpol.2017.10.122>, 2018b.
- 515 Wang, P., Chen, Y., Hu, J., Zhang, H., and Ying, Q.: Source apportionment of summertime ozone in China using a source-oriented chemical transport model, *Atmos. Environ.*, 211, 79-90, <https://doi.org/10.1016/j.atmosenv.2019.05.006>, 2019.
- Wang, Y., Zhao, Y., Zhang, L., Zhang, J., and Liu, Y.: Modified regional biogenic VOC emissions with actual ozone stress and integrated land cover information: A case study in Yangtze River Delta, China, *Sci. Total. Environ.*, 727, 10.1016/j.scitotenv.2020.138703, 2020.
- 520 Wu, K., Yang, X., Chen, D., Gu, S., Lu, Y., Jiang, Q., Wang, K., Ou, Y., Qian, Y., Shao, P., and Lu, S.: Estimation of biogenic VOC emissions and their corresponding impact on ozone and secondary organic aerosol formation in China, *Atmos. Res.*, 231, 104656, <https://doi.org/10.1016/j.atmosres.2019.104656>, 2020.
- Xiao, Z., Liang, S., Wang, J., Chen, P., Yin, X., Zhang, L., and Song, J.: Use of General Regression Neural Networks for Generating the GLASS Leaf Area Index Product From Time-Series MODIS Surface Reflectance, *IEEE Trans Geosci. Remote Sens.*, 52, 209-223, 10.1109/TGRS.2013.2237780, 2014.
- 525 Xiao, Z., Liang, S., Wang, J., Xiang, Y., Zhao, X., and Song, J.: Long-Time-Series Global Land Surface Satellite Leaf Area Index Product Derived From MODIS and AVHRR Surface Reflectance, *IEEE Trans Geosci. Remote Sens.*, 54, 5301-5318, 10.1109/TGRS.2016.2560522, 2016.
- 530 Ying, Q., Li, J., and Kota, S. H.: Significant Contributions of Isoprene to Summertime Secondary Organic Aerosol in Eastern United States, *Environ. Sci. Technol.*, 49, 7834-7842, 10.1021/acs.est.5b02514, 2015.
- Zhang, H., and Ying, Q.: Secondary organic aerosol formation and source apportionment in Southeast Texas, *Atmos. Environ.*, 45, 3217-3227, <https://doi.org/10.1016/j.atmosenv.2011.03.046>, 2011.



- 535 Zhang, H., Li, J., Ying, Q., Yu, J. Z., Wu, D., Cheng, Y., He, K., and Jiang, J.: Source apportionment of PM_{2.5} nitrate and sulfate in China using a source-oriented chemical transport model, *Atmos. Environ.*, 62, 228-242, <https://doi.org/10.1016/j.atmosenv.2012.08.014>, 2012.
- Zhang, R., Cohan, A., Biazar, A. P., and Cohan, D. S.: Source apportionment of biogenic contributions to ozone formation over the United States, *Atmos. Environ.*, 164, 8-19, [10.1016/j.atmosenv.2017.05.044](https://doi.org/10.1016/j.atmosenv.2017.05.044), 2017.
- Zhang, X., Cappa, C. D., Jathar, S. H., McVay, R. C., Ensberg, J. J., Kleeman, M. J., and Seinfeld, J. H.: Influence of vapor wall loss in laboratory chambers on yields of secondary organic aerosol, *Proc. Nat. Acad. Sci.*, 111, 5802-5807, [10.1073/pnas.1404727111](https://doi.org/10.1073/pnas.1404727111), 2014.
- 540 Zhang, Y. L., Zhang, R. X., Yu, J. Z., Zhang, Z., Yang, W. Q., Zhang, H. N., Lyu, S. J., Wang, Y. S., Dai, W., Wang, Y. H., and Wang, X. M.: Isoprene Mixing Ratios Measured at Twenty Sites in China During 2012-2014: Comparison With Model Simulation, *J. Geophys. Res. Atmos.*, 125, [10.1029/2020JD033523](https://doi.org/10.1029/2020JD033523), 2020.
- Zhao, C., Wang, Y., Yang, Q., Fu, R., Cunnold, D., and Choi, Y.: Impact of East Asian summer monsoon on the air quality over China: View from space, *J. Geophys. Res. Atmos.*, 115, <https://doi.org/10.1029/2009JD012745>, 2010.
- 545 Zhao, C., Huang, M. Y., Fast, J. D., Berg, L. K., Qian, Y., Guenther, A., Gu, D. S., Shrivastava, M., Liu, Y., Walters, S., Pfister, G., Jin, J. M., Shilling, J. E., and Warneke, C.: Sensitivity of biogenic volatile organic compounds to land surface parameterizations and vegetation distributions in California, *Geosci. Model Dev.*, 9, 1959-1976, [10.5194/gmd-9-1959-2016](https://doi.org/10.5194/gmd-9-1959-2016), 2016.



550

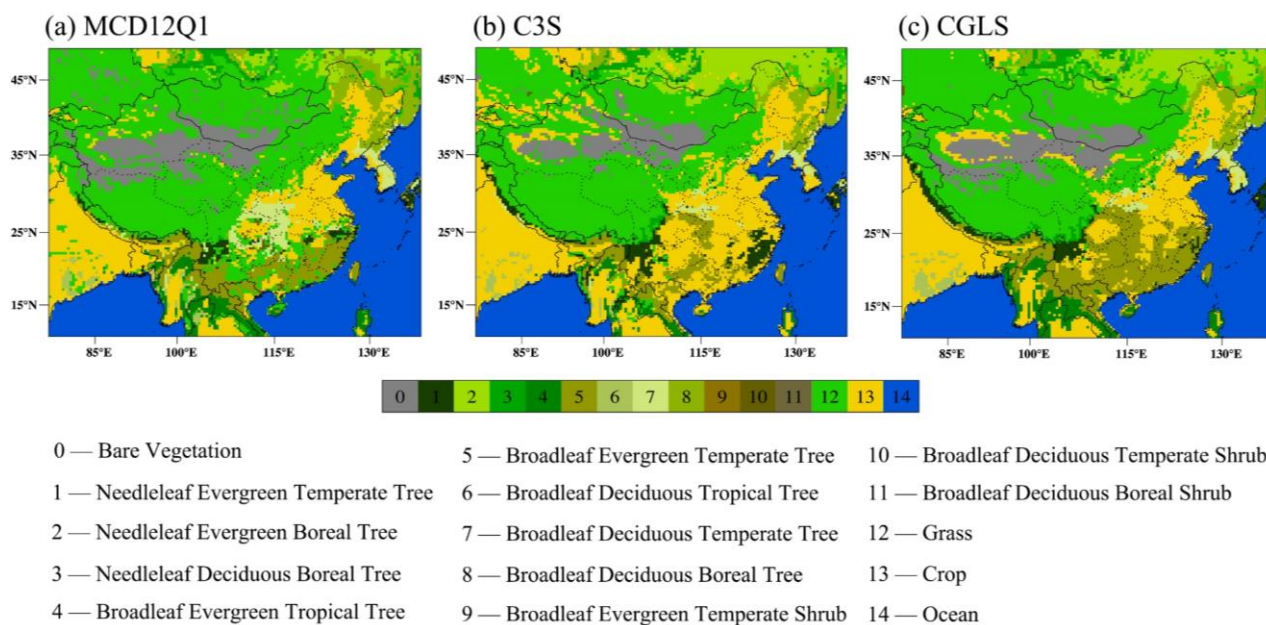
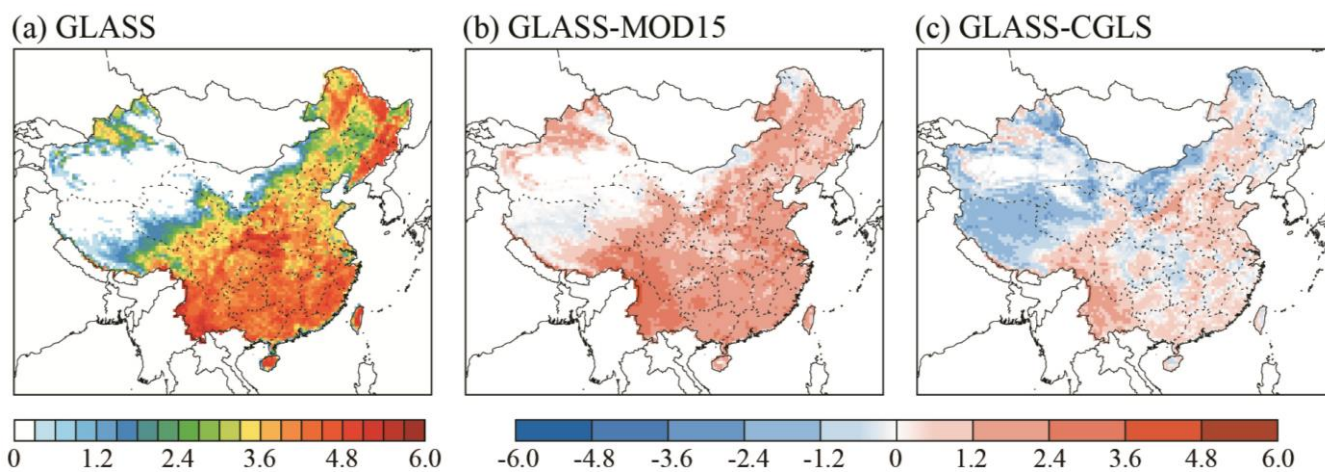


Figure 1. Simulation domain with the spatial distribution of majority PFTs in each grid.



555 Figure 2. Distribution of LAIv from different satellite datasets in the summer of 2016.

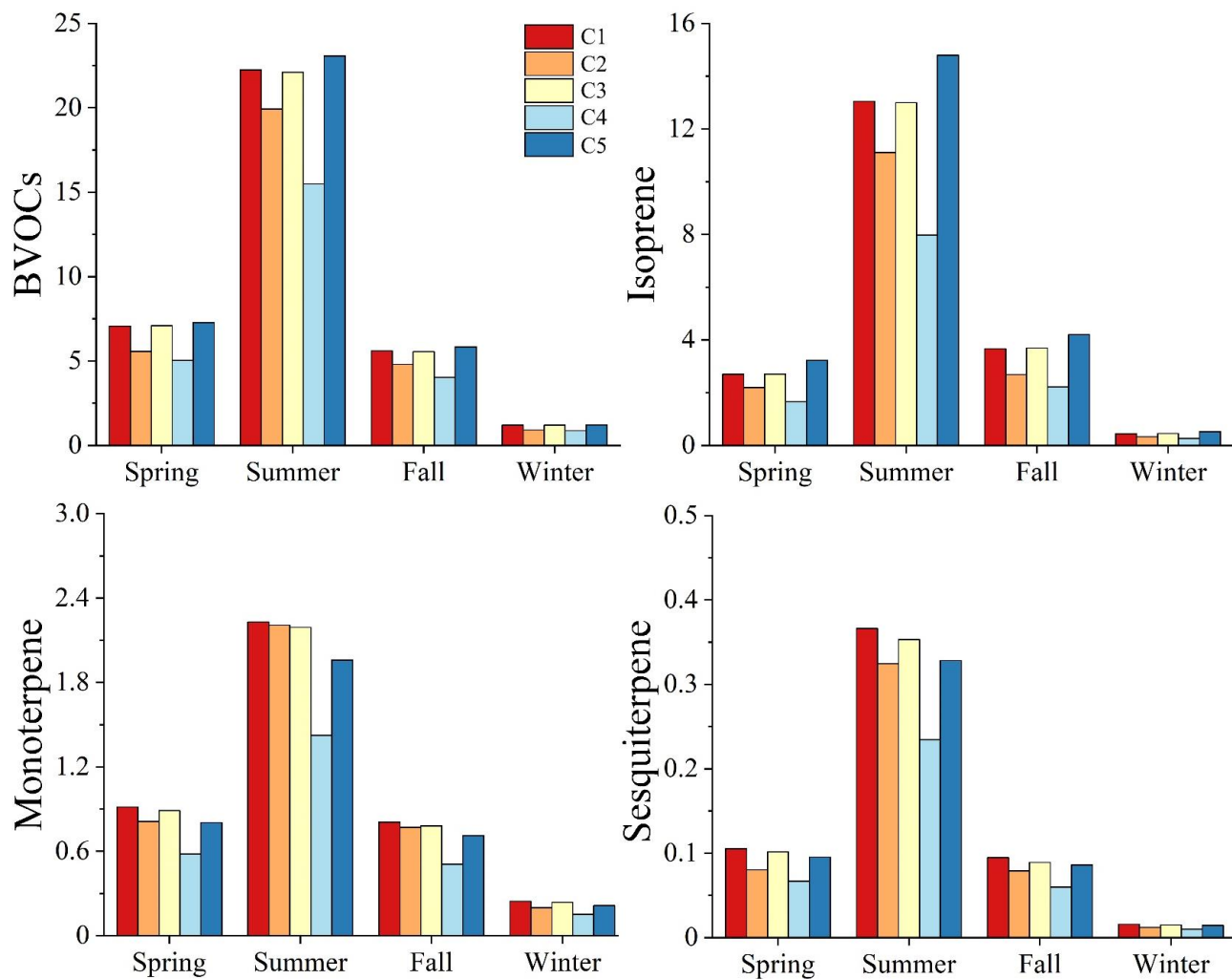


Figure 3. Seasonal emissions of isoprene, monoterpenes, sesquiterpenes, and total BVOCs of each case in China. Unit is Tg.

560

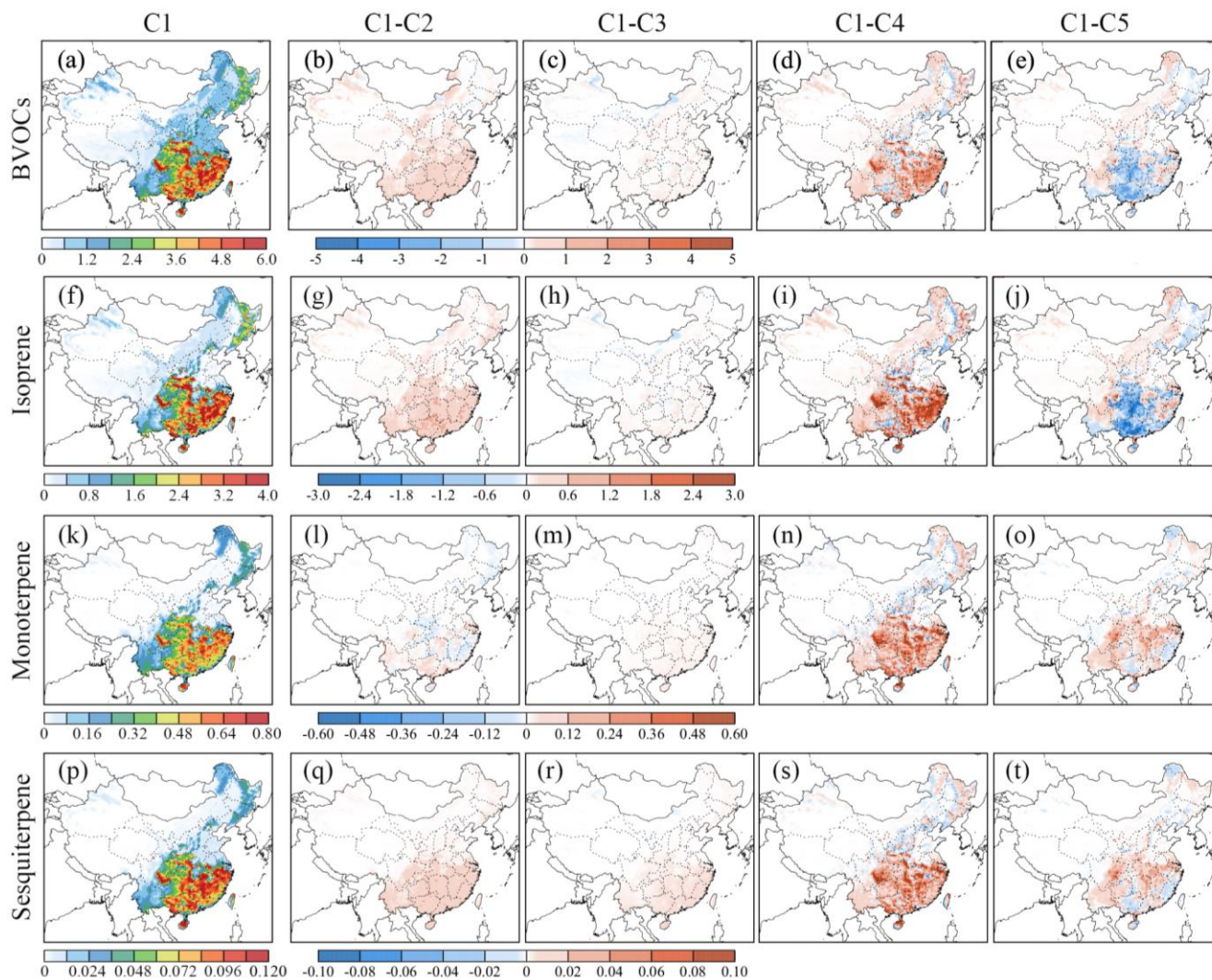


Figure 4. Comparison of three main BVOC species in different cases in summer (June, July and August) ((a), (f), (k), and (p): C1; (b), (g), (l), and (q): C1-C2; (c), (h), (m), and (r): C1-C3; (d), (i), (n), and (s): C1-C4; (e), (j), (o), and (t): C1-C5). Unit is $\text{mg m}^{-2} \text{h}^{-1}$.

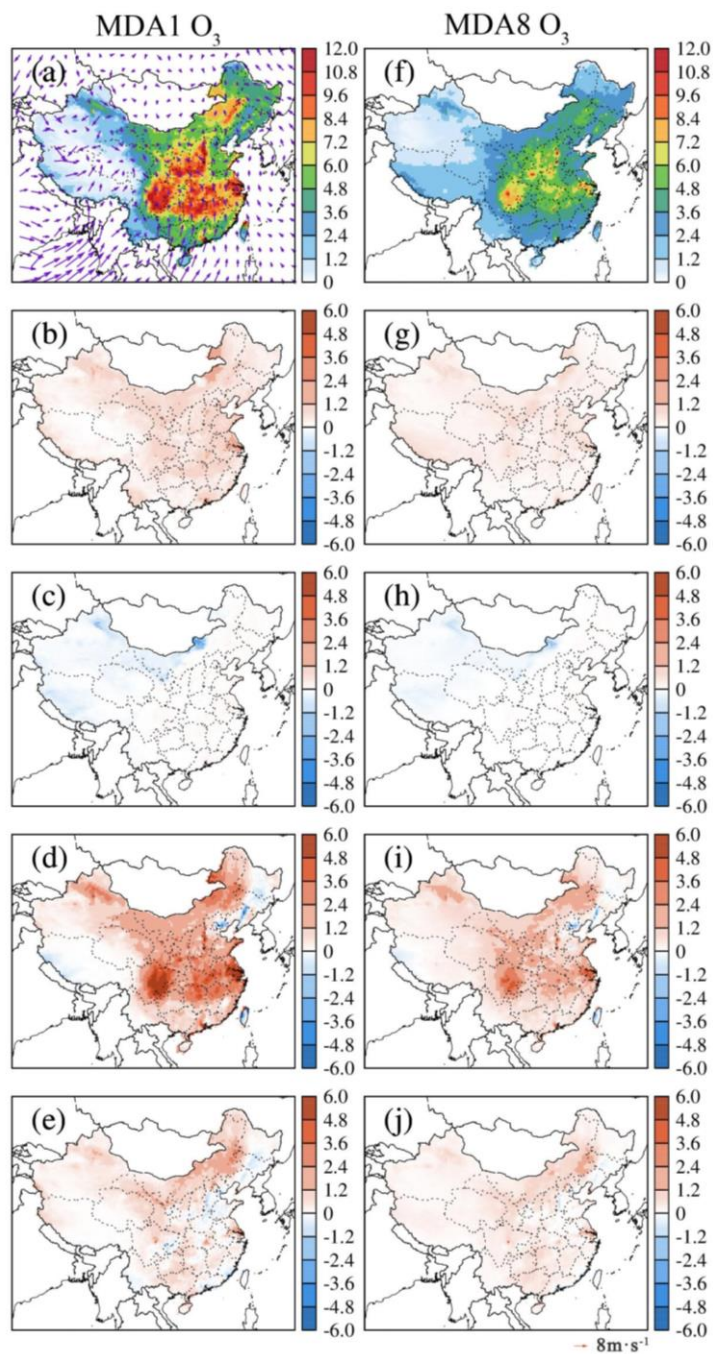
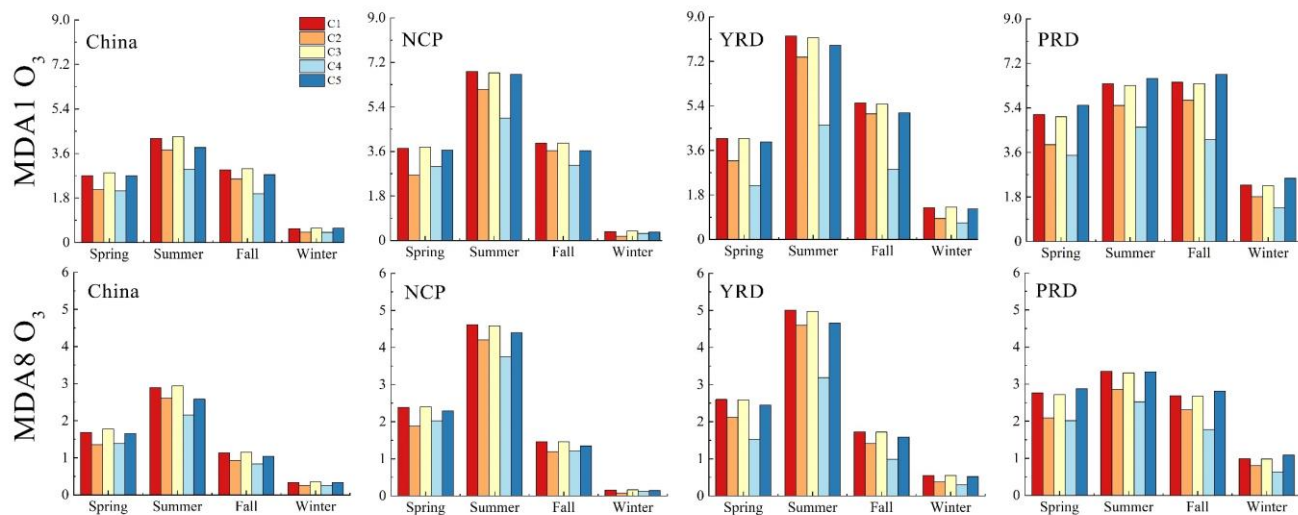
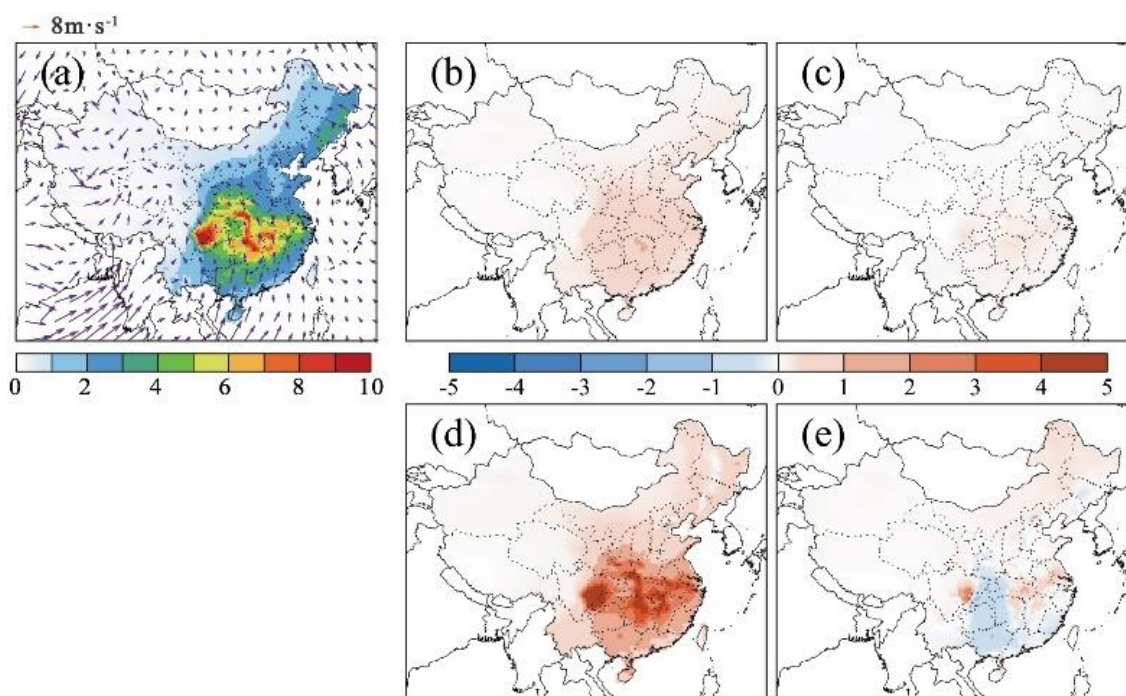


Figure 5. Spatial distributions of MDA1 O₃ and MDA8 O₃ from biogenic source in different cases in summer ((a) and (f): C1, (b) and (g): C1-C2, (c) and (h): C1-C3, (d) and (i): C1-C4, (e) and (j): C1-C5). Unit is ppb.



570 **Figure 6. Seasonal averaged concentrations of MDA1 O₃ and MDA8 O₃ from biogenic emissions in important regions and China.**



575 **Figure 7. Spatial distributions of simulated SOA from biogenic source in different cases in summer. Unit is $\mu\text{g m}^{-3}$ ((a): C1, (b): C1-C2, (c): C1-C3, (d): C1-C4, (e): C1-C5).**

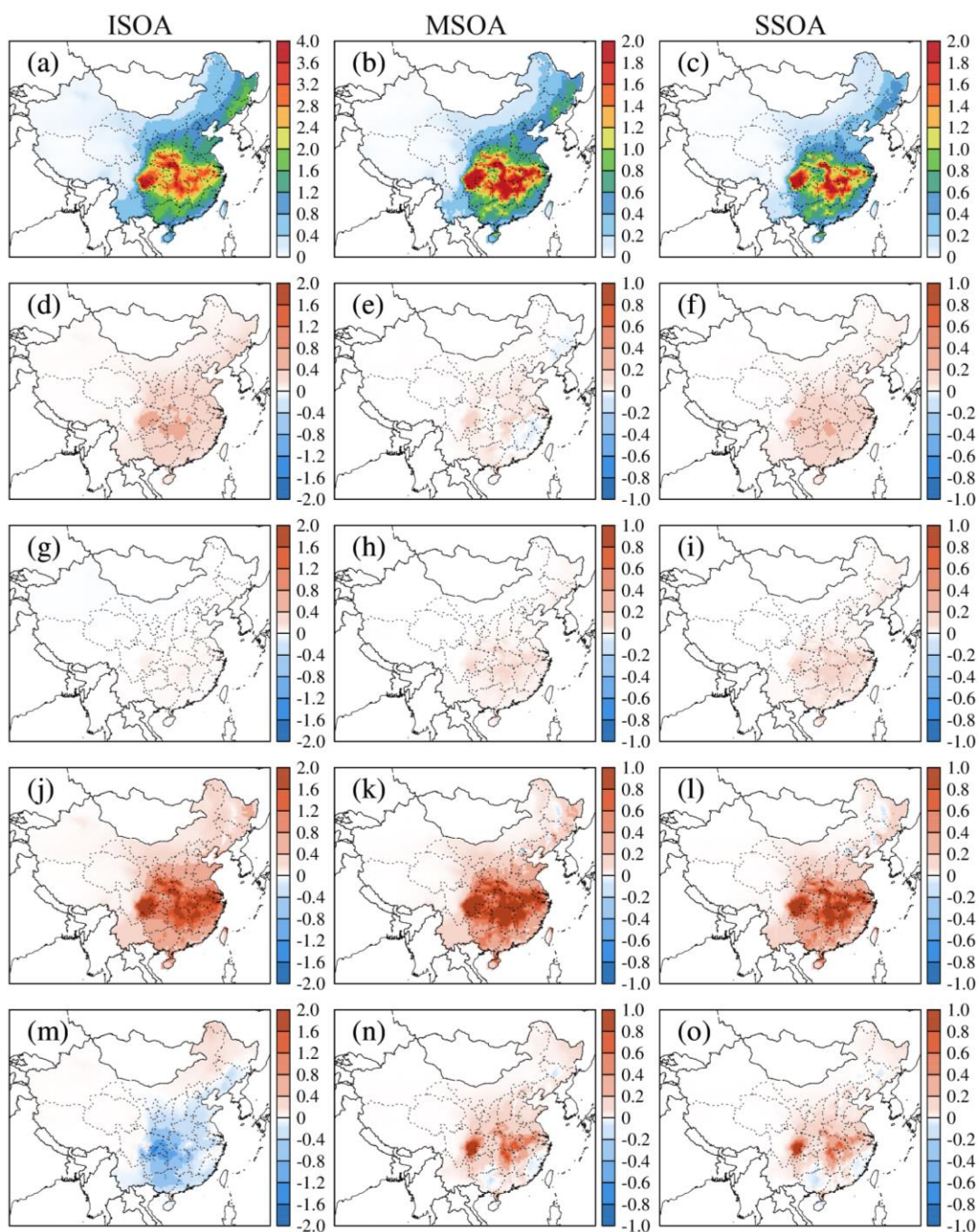


Figure 8. Spatial distributions of simulated SOA from isoprene (ISOA), monoterpenes (MSOA), and sesquiterpenes (SSOA) in different cases in summer ((a), (b), and (c): C1; (d), (e), and (f): C1-C2; (g), (h), and (i): C1-C3; (j), (k), and (l): C1-C4; (m), (n), and (o): C1-C5). Unit is $\mu\text{g m}^{-3}$.

580

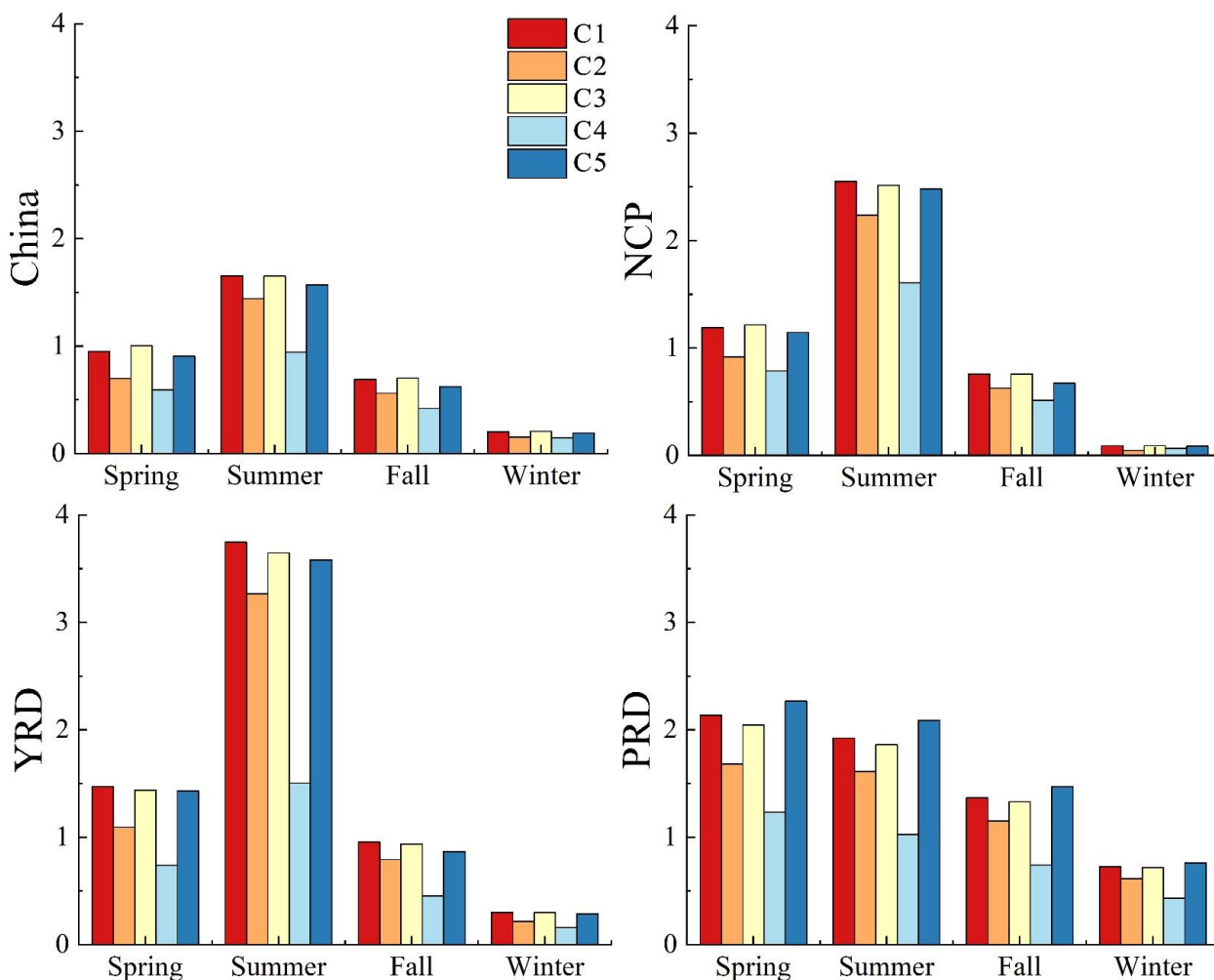


Figure 9. Seasonal distributions of biogenic SOA (BSOA) for all cases in important regions and China. Unit is $\mu\text{g m}^{-3}$.



585

Table 1. Simulation schemes with different land cover (LC) and leaf area index (LAI).

Case	BVOCs		Description
	LC	LAI	
C1	MCD12Q1	GLASS	As baseline
C2	MCD12Q1	MOD15	Compared to C1, accounts for LAI difference between GLASS and MOD15
C3	MCD12Q1	CGLS	Compared to C1, accounts for LAI difference between GLASS and CGLS
C4	C3S LC	GLASS	Compared to C1, accounts for LC difference between MCD12Q1 and C3S LC
C5	CGLS LC	GLASS	Compared to C1, accounts for LC difference between MCD12Q1 and CGLS LC

Table 2. The area fraction of different plant function types (PFTs) in China from three land cover satellite datasets.

Datasets	Broadleaf trees	Needleleaf trees	Shrub	Grass	Crop
MCD12Q1	12.9 %	5.0 %	5.1 %	33.9 %	13.9 %
CGLS LC	16.4 %	4.6 %	0.3 %	19.4 %	17.8 %
C3S LC	9.2 %	4.9 %	2.3 %	20.9 %	23.6 %

590 **Table 3. Estimated BVOC emissions (Tg) in different cases across China.**

	C1	C2	C3	C4	C5
Isoprene	19.84	16.32	19.83	12.10	22.73
Monoterpenes	4.19	3.99	4.10	2.66	3.69
Sesquiterpenes	0.58	0.50	0.56	0.37	0.52
Other VOCs	11.49	10.42	11.46	10.29	10.45
Total	36.10	31.22	35.94	25.42	37.39

Table 4. Previous studies of BVOC emissions estimated using MEGAN in China, unit is Tg yr⁻¹.

Reference	Year	LAI	PFT	Isoprene	Monoterpenes	Total BVOCs
Wang et al. (2021)	2016	MODIS MOD15A2H	MODIS MCD12C1	16.70	4.12	35.48
Wu et al. (2020)	2017	MODIS MOD15A2H	MODIS MCD12Q1	13.30	3.09	23.54
Li et al. (2020)	2018	MEGAN-L database	Vegetation Atlas	37.45	6.69	58.89
Stavrakou et al. (2014)	1979- 2012	MODIS MOD15A2H	Default MEGAN map with the updated cropland map	9.30	\	\
Li et al. (2013)	2003	Biomass-apportion models results	Vegetation Atlas	20.70	4.90	42.50
Fu and Liao (2012)	2001- 2006	MODIS MOD15A2H	MODIS MCD12Q1	9.59	2.83	18.85